ACS Sustainable Chemistry & Engineering

pubs.acs.org/journal/ascecg

Research Article

Biopolymers Fractionation and Synthesis of Nanocellulose/Silica Nanoparticles from Agricultural Byproducts

Naresh Shahi, Pixiang Wang, Sushil Adhikari, Byungjin Min,* and Vijaya K. Rangari*

Cite This: https://doi.org/10.1021/acssuschemeng.0c09342

Read Online

ACCESS | Metrics & More | Article Recommendations | Supporting Information

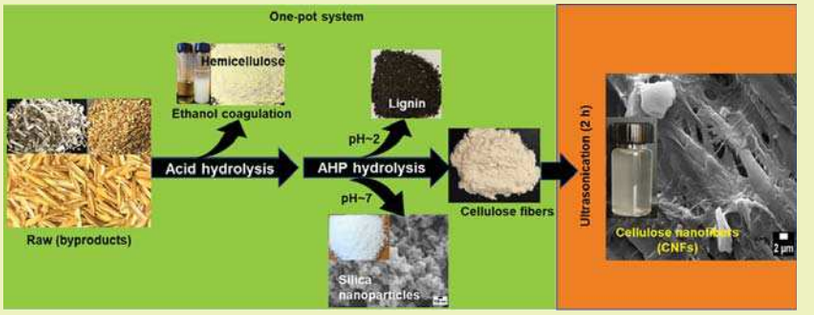

ABSTRACT: Agricultural byproducts rich in lignocellulose are considered one of the most promising feedstocks to produce sustainable value-added materials with different industrial applications. However, fractionation into carbohydrates, lignin, and silica is a key challenge in the conversion of plant biomass into value-added products due to its complex structure. This study is designed to develop a novel method for sequential separation and collection of cellulose, hemicellulose, lignin, and silica from agricultural byproducts, peanut shell (PS), rice husk (RH), and sugar cane bagasse (SB), using an integrated approach under mild hydrolysis conditions. Silica and cellulose nanofibers (CNFs) were synthesized using an ultrasonic-assisted chemical method. Pure silica was obtained by further pyrolysis. The yield percent of cellulose was 35%, 39%, and 41% and hemicellulose and lignin combined was 30%, 18%, and 29% from PS, RH, and SB, respectively. The X-ray diffraction results demonstrated that CNFs were semicrystalline from all samples, and CNFs from SB had the highest crystallinity. Similarly, silica nanoparticles (SNPs) were amorphous in RH, while it was crystalline in both PS and SB. The surface morphologies of the CNFs and nanosized fibers were observed by field emission-scanning electron microscopy. It revealed that there were different morphological characteristics such as web-like, parallel, and tangled in PS, RH, and SB, respectively. The surface morphology of SNPs was also varied among the samples. In BET analysis, SNPs from RH had a larger specific surface area of 37.5 m^2/g and total pore volume of 0.08 cc/g compared to SNPs from both PS and SB. The ascribed method could be a potential approach for comprehensive utilization of agricultural biomass through a relatively simple process, which can then be used for the biorefinery process or as a feedstock for the biomaterials industry. It is also suggested that the structural variations of CNFs/SNPs might be a vital factor to be considered for selecting optimal biomaterials.

KEYWORDS: *Agricultural byproducts, Biomaterials, Nanocellulose, Silica*

INTRODUCTION

Lignocellulosic biomass is renewable, biocompatible, and abundant on earth. Thus, extensive research has been conducted on the utilization of lignocellulose for biobased commercial products such as bioplastics, biomaterials, biochemicals, and advanced biofuels.[1−3] Agricultural byproducts such as peanut shell (PS), rice husk (RH), and sugar cane bagasse (SB) are rich in lignocellulose, available year round, and low-value residues that are left over after the extraction of consumable parts generated from the milling processes.[4] The lignocellulose consists of cellulose (40−50%), hemicellulose (20−40%), and lignin (20−30%). Techniques have been described to separate them for the synthesis of nanocellulose, nanohemicellulose, and nanolignin with divergent and controllable properties.[2] In addition to lignocellulose, agricultural byproducts also contain silica. For instance, RH contains 15−28 wt % of silica.[5] Therefore, this study aimed to extract both lignocellulose and silica from agricultural byproducts.

Among the lignocellulosic components, cellulose is a significant portion of the plant biomass, and a homogeneous polymer consists of glucose monomers. Cellulose can be transformed into cellulose nanofibers (CNFs) and cellulose

Received: December 27, 2020
Revised: April 7, 2021

nanocrystals (CNCs). In general, these two forms are demanding nanocellulose due to their unique properties such as nanodimension in size, large surface area, low density, high strength, high-temperature resistance, and biocompatibility.[6] Due to the superior properties of nanocellulose, it could be an excellent candidate in a wide range of applications such as food packaging materials, biofuels, electronic devices, and pharmaceuticals.[2,7] Hemicellulose is a heterogeneous polymer composed of xylans, galactoses, arabinans, and mannans. Hemicellulose and its derivatives are precursors of biofuels, organic acids, sugar alcohols, olefins, and furans.[8] It can also serve as a direct substrate for preparing thin films, coating materials, and hydrogel.[9,10] Similarly, lignin is a complex structure composed of cross-linked polymers of phenolic monomers. It is widely used in industrial commodities such as fuels, aromatics, carbon fiber, adhesive, resins, and dispersant.[11] Likewise, silica is a valuable inorganic multipurpose chemical compound with a projected $8.8 billion market in 2020.[12] Silica nanoparticles have a wide range of applications in paints, Li-ion batteries, catalysts, and adsorbents.[5] Silica nanoparticles produced from agroindustrial waste have been used as green absorbents because of the high degree of porosity and high surface area, making it easy to physically adsorb heavy metals (Hg, Pb, Ni, Cu) and chemicals contaminants.[13] Moreover, the commonly used silica precursor, tetraethyl orthosilicate, is more expensive; hence, agricultural wastes that include silica are used as an alternative.[14] Individual lignocellulosic components and silica from plant biomass could be assembled into a functional composite membrane for filtration of solute particles and gases. For example, Kauldhar et al. developed a flexible composite membrane from cellulose nanofibers, nanosized silica, and lignin isolated from sugar cane bagasse for water purification.[15] Therefore, it is of tremendous environmental and economic advantage to utilize both lignocellulosic components and silica from agricultural byproducts.

Several techniques have been studied to isolate lignocellulosic constituents and silica from plant biomass, including physical, chemical, and biological methods. The chemical method, basically alkali combined with hydrogen peroxide, has been extensively used to fractionate lignocellulosic components. The main benefit of alkaline hydrogen peroxide (AHP) pretreatment is the selective separation of lignocellulosic components from plant biomass and limiting sugar loss via the degradation process.[16,17] Researchers have also contributed to the development of AHP treatment and separation of lignocellulosic components, including silica, from plant biomass.[18−21] For example, Mittal et al. reported that more than 80% of the lignin could be removed from corn stover.[18] According to Alvarez-Vasco, AHP pretreatment of softwood could remove a significant amount of lignin (22%) and glucomannan (78%) in weight percentage without cellulose degradation.[19] As mentioned by Abd-Talib et al., AHP treatment resulted in 84% silica removal, 80% delignification, and 8% reduced sugar production from rice straw.[20] Our research team also isolated cellulose and produced cellulose nanofibers using a combination of AHP and ultrasonication techniques from cover crops and sugar cane bagasse.[22,23] However, our previous studies were mainly focused on the extraction of individual carbohydrates and lignin rather than the complete utilization of lignocellulosic components and silica as a whole. Therefore, a feasible approach is indispensable to isolate and recover valuable components to maximize consumption and capitalize on agricultural byproducts.

In this study, lignocellulosic components were separated and synthesized cellulose nanofibers (CNFs)/silica nanoparticles (SNPs) from agricultural byproducts such as peanut shell, rice husk, and sugar cane bagasse in the integrated reaction system using an ultrasonic-assisted chemical method. During the extraction process, mild sulfuric acid treatment was employed for hemicellulose, and the AHP solution coupled with ultrasonication was employed for lignin and silica. Extracted lignocellulosic components were quantified and examined for their structural properties. In parallel, the physical and thermal properties of the synthesized CNFs and SNPs were investigated. On the basis of our knowledge, the method used in this study is the first of its kind for the comprehensive use of agricultural wastes by deriving lignocellulosic components and silica.

EXPERIMENTAL SECTION

Materials and Reagents. Agricultural byproducts peanut shell (PS), rice husk (RH), and sugar cane bagasse (SB) were used as the sources for lignocellulose and silica. The PS and SB were obtained from the George Washington Carver Agricultural Experimental Station, Tuskegee University, AL, and RH from Three H's, LLC Crossett, AR. Sulfuric acid, sodium hydroxide, hydrogen peroxide, and ethanol were purchased from Sigma-Aldrich, Millipore Sigma, St. Louis, MI. Commercial cellulose nanocrystals (CNCs, lot no. 2015-FPL-CNC-077) and cellulose nanofibers (CNFs, lot no. U37) were purchased from the University of Maine, Process Development Center, Maine, USA. Commercial nanocelluloses were used to compare the crystallinity of our isolated nanocellulose. A ground powder of PS, RH, and SB was further disintegrated into a fine powder using a ball mill for 2 h. Milling is employed to reduce the particle size of the samples and crystallinity, which leads to high surface contact and a high pore volume of the plant biomass.[24] Conversely, the ultrafine powder (<25 μm) form of biomass possesses modified physicochemical properties that exposed and increased the inner surface with high cellulose/hemicellulose components at the surface.[25−27] However, a biomass particle size less than 0.4 mm has no remarkable effect on the hydrolysis rate and yield.[28] In our study, the milled powder samples were sieved through 0.50 mm diameter mesh to collect the homogeneous particles for further analysis.

Lignocellulose and Silica Extraction. The major components, cellulose, hemicellulose, lignin, and silica, were isolated through three sequential steps in the integrated one-pot reaction system. The yield percentage was reported compared with the original raw sample mass. In the first step, 5 g of homogeneous dry powder from selected biomass was added to a flask containing 50 mL of 0.1 M sulfuric acid. The solution was continuously stirred at 75 ± 5 °C for 2 h. After the designated time, the solids and liquid portions were filter using a vacuum pump. The solid portion contained cellulose, lignin, and silica, while the filtrate was hemicellulose and inorganic minerals such as iron. The dissolved hemicellulose was concentrated using a rotary evaporator. The concentrated solution was recovered by coagulation in ethanol (100%) by keeping it for 12 h at room temperature and harvested with centrifugation at 4500 rpm for 5 min. Collected hemicellulose was dried in an oven at 50 °C for 12 h. The pretreated pulp was washed several times with DI water until the filtrate achieved neutral pH. The neutralized pulp was dried at 105 °C for 2 h for further analysis.

In the second step, the neutralized pulp after acid hydrolysis was used to extract lignin and silica using an alkaline hydrogen peroxide (AHP) solution at high pH (~11.05) using an ultrasonic bath for 2 h at 50 ± 2 °C. After the designated time, the dissolved black liquor containing lignin and silica was collected by vacuum filtration. Dissolved lignin and silica were recovered by acid coagulation using 5 M sulfuric acid at different pHs. Silica was precipitated at around pH 6.5−7, and the sample was then refrigerated for 12 h for

https://doi.org/10.1021/acssuschemeng.0c09342
ACS Sustainable Chem. Eng. XXXX, XXX, XXX−XXX

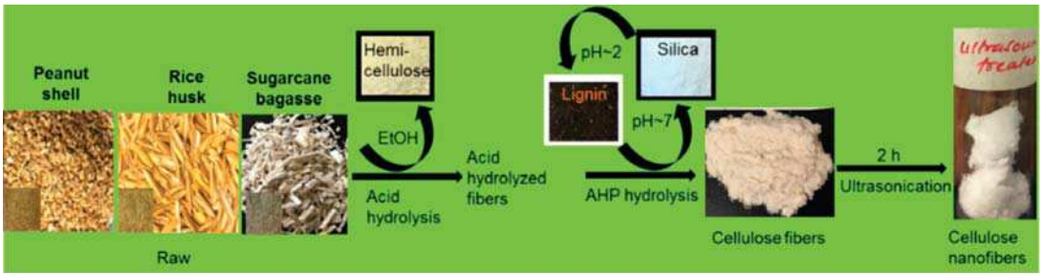

Figure 1. Extraction process of cellulose, hemicellulose, lignin, silica, and cellulose nanofibers in the integrated "one-pot" system from agricultural byproducts (peanut shell, rice husk, and sugar cane bagasse). Inserted images in the raw samples are a ball-milled fine powder.

sedimentation. After the coagulation period, the white residue was recovered by centrifugation at 4500 rpm for 10 min. The recovered residue was pyrolyzed at 700 °C for 2 h; this heating process at high temperature removed organic impurities and left behind silica powder. Silica powders were confirmed to be silica nanoparticles (SNPs) by investigating its structural morphology, as discussed in the Results and Discussion. The supernatant from the remaining solution was collected and acidified further down to pH ≈ 2 for lignin coagulation. The sedimented lignin at the refrigerated temperature for 12 h was collected and purified by centrifugation at 4500 rpm for 5 min. The harvested lignin was neutralized in cellulose tubing by replacing the water every 24 h for 3 days. In the final step, undissolved cellulose pulp was collected to produce nanocellulose using an ultrasonic probe. The isolation process along with hemicellulose, lignin, and silica images are available in the Supporting Information (Figure S1). In the extraction process, three samples were tested from each sample, and the average values are reported.

Cellulose Transforms into Nanocellulose. Nanocellulose was produced from AHP-treated cellulose fibers using the ultrasonic-chemical method. Details of the methodology and morphology of the synthesized cellulose can be found in a previous study.[22] In brief, cellulose pulp was irradiated using an (frequency, 20 kHz) ultrasonic titanium horn (probe tip of diameter 13 mm) for 2 h. The output power of the ultrasound irradiation was set at 750 W with an amplitude of 70%. The obtained slurry was centrifuged to remove the excess water at 10 000 rpm for 10 min at 4 °C and dried in an oven at 60 °C for 12 h. This sample was used for further characterization.

Composition Analysis. Structural carbohydrates (cellulose and hemicellulose) and lignin of biomass were determined according to the US National Renewable Energy Laboratory (NREL) protocol.[29] Briefly, 0.3 g of oven-dried residue was acidified in 72% sulfuric acid (3 mL) at 30 °C for 1 h. After completion of acid hydrolysis, the samples were diluted to 4% concentration by adding ∼84 mL of deionized water, and the samples were autoclaved at 121 °C for 1 h. The dissolved aliquot was collected using a vacuum filter for sugars and acid-soluble lignin analysis, while the undissolved portion (filtration residue) was used to determine acid-insoluble lignin by weight percentage. For the dissolved aliquot, acid-soluble lignin was determined using UV−vis spectrophotometer measurement (HACH, DR600, Germany), and sugars were determined by an Agilent 1260 high-performance liquid chromatography (HPLC) system (Agilent Technology, CA). The HPLC system was equipped with a refractive index detector (RID), a 300 mm × 7.8 mm (i.d.), 9 μm Aminex HPX-87P column, and a 30 mm × 4.6 mm (i.d.) guard column (Bio-Rad, Hercules, CA). Nanopure water was used as the mobile phase at an isocratic flow rate of 0.6 mL/min, and the temperature was maintained at 80 °C during the 20 min elution. The results are reported as the mean of three runs from each sample with their standard deviation.

Ash Determination. The ash content was determined by following the NREL method using a muffle furnace (F47915, Barnstead International, USA).[30] In the method, an empty, clean crucible was first heated to constant weight. Around 1 g of oven-dried samples was placed in the crucible and incinerated at 575 ± °C for 24 ± 2 h. Weight was recorded in triplicate after cooling at room temperature to analyze the ash content.

Characterization. The structural property, surface morphology, and thermal stability of the synthesized nanocellulose and silica were compared. Scanning electron microscopy images were acquired on a field emission-scanning electron microscope (FE-SEM) equipped with an energy-dispersive X-ray spectrometer (Joel-JEM-7200F, Japan). All samples were sputtered coated with a thin layer of Au/Pd before SEM imaging. Image evaluation was carried out using the ImageJ software and reported in Supporting Information Figure S6. The silica purity and presence were measured in the energy-dispersive spectrum (EDS), which was collected during FE-SEM imaging. The X-ray diffraction (XRD) pattern was recorded using a wide-angle XRD Rigaku DMAX 2100 diffractometer containing monochromatic Cu Kα radiation (λ = 0.154 nm) at 40 kV and 30 mA. Diffracted radiation was collected in the range from 10° to 50° at a speed of 2θ 2°/min. The as-extracted cellulose nanofibers crystallinity was compared with commercial cellulose nanocrystals (CNCs) and cellulose nanofibers (CNFs). The intensity of crystallinity was determined by the peak height method. The XRD data was analyzed using MDI JADE software (version 7.8.2, MDI). Fourier transform infrared spectroscopy (FTIR) using a Nicolet, Nexus model 670/680, Thermo Electron Corp., USA, equipped with a universal attenuated total reflection (ATR) probe and Raman spectroscopy (DXR, Thermo Scientific, USA) equipped with 780 nm wavelength laser were used to analyze the chemical components of the samples. The specific surface area measurements were performed using the Brunauer−Emmett−Teller (BET) surface area and a porosity analyzer (Quantachrome Instruments, autosorb iQ, Boynton Beach, FL, USA). The samples were degassed at 300 °C with a continuous flow of helium for 16 h. Samples were then placed in the analyzer, and nitrogen was used as the adsorbate gas to measure the surface area.[31] Thermal gravimetric analysis (TGA) was carried out with a TA Instruments TGA Q500 series. The degradation temperature was analyzed using Origin Pro 2021 (student version) software. Approximately 10 mg of samples was placed on the platinum pan of a TA Instruments device. Samples were heated from 30 to 600 °C at a constant heating rate of 10 °C/min under a nitrogen atmosphere with a purge rate of 20 mL/min. All of the TGA results are reported as an average of three repetitions of different samples.

RESULTS AND DISCUSSION

Lignocellulose and Silica Extraction. Sequential extraction was performed in the integrated one-pot reaction system to separate cellulose, hemicellulose, lignin, and silica. Visual macroscopic evaluation of the samples after each stage of treatment is presented in Figure 1. In particular, the first step in the isolation process was to separate hemicellulose. It was recovered in ethanol coagulation; sediments were harvested and dried to obtain a milky white powder "hemicellulose" as the end product (see Figure 1 and Figure S1). The recovered weight percentages of hemicellulose from PS, RH, and SB were 20%, 16%, and 19%, respectively, from the original sample. Hemicellulose extracted by acid leaching and alkaline treat-

https://doi.org/10.1021/acssuschemeng.0c09342
ACS Sustainable Chem. Eng. XXXX, XXX, XXX−XXX

Table 1. Concentration (%) of Lignocellulosic Components and Silica from PS, RH, and SB by HPLC Analysis[a]

sample	glucose	xylan	galactan	arabinan	manan	lignin	silica
raw-PS	31.4 ± 1.1	10.1 ± 1.2	5.2 ± 0.6	2.2 ± 0.5	3.9 ± 0.2	35.1 ± 2.2	
cellulose-PS	61.4 ± 1.2	1.4 ± 0.0	1.4 ± 0.2	1.5 ± 0.3	1.6 ± 0.0	19.1 ± 1.3	10.8 ± 1.0
CNF-PS	76.0 ± 2.2	0.9 ± 0.1	1.2 ± 0.0	1.2 ± 0.2	1.6 ± 0.0	9.0 ± 0.5	
raw-RH	35.1 ± 0.8	9.2 ± 0.1	3.3 ± 0.2	2.3 ± 0.0	3.1 ± 0.0	23.8 ± 2.3	
cellulose-RH	61.8 ± 1.1	3.1 ± 0.0	1.3 ± 0.1	0.7 ± 0.3	3.2 ± 0.0	12.5 ± 1.1	20.0 ± 0.2
CNF-RH	70.7 ± 2.2	1.9 ± 0.01	0.0 ± 0.0	0.6 ± 0.0	3.0 ± 0.0	5.5 ± 0.2	
raw-SB	39.7 ± 1.8	8.0 ± 0.2	6.4 ± 0.7	2.9 ± 0.6	4.0 ± 0.1	30.4 ± 1.3	
cellulose-SB	75.9 ± 1.1	2.5 ± 0.0	1.0 ± 0.0	2.2 ± 0.3	1.3 ± 0.0	2.4 ± 0.2	7.0 ± 1.0
CNF-SB	83.8 ± 1.8	1.1 ± 0.1	1.0 ± 0.0	0.3.0 ± 0.1	1.4.0 ± 0.2	0.5 ± 0.0	

[a]Abbreviations: PS, RH, SB, and CNFs represent peanut shell, rice husk, sugar cane bagasse, and cellulose nanofibers, respectively. (±) is standard deviation from treatment replication.

ment and recovered in ethanol precipitation was about 28% w/w from 55% w/w of the original hemicellulose content in giant cane (*Arundo donax*).[32]

In the second step, the combined dark brown alkali filtrate was precipitated and separated silica (pH ≈ 7) and lignin (pH ≈ 2) from each sample by changing the solution's pH. The precipitated residue is concentrated and dried. The obtained products were bright white and black powder, labeled as silica and lignin, respectively. Silica from PS, RH, and SB was precipitated and purified from the neutralized solution before lignin coagulation. The collected silica was further processed for pyrolysis at 700 °C for 2 h to produce pure white powder silica. A visual macroscopic image of silica after pyrolysis is also shown in Figure 1; percent yields by weight were 10%, 20%, and 7% from PS, RH, and SB, respectively. The change in color from a brown to a white powder is due to the combustion of impurities such as lignocellulose (Figure S1). The observed white powder was further confirmed and compared among the samples as silica nanoparticles (SNPs) by the FE-SEM and EDS results. The percent lignin recovered after dialysis and oven-dried weight was around 31%, 24%, and 25% from PS, RH, and SB. The undissolved pulp was dried to obtain cellulose-rich fibers (see Figure 1). The cellulose yield was 35%, 39%, and 41% from PS, RH, and SB, respectively. The untreated sample color was brown and turned white upon treatment in an ultrasonic bath using the AHP solution. These color changes are due to the removal of noncellulosic materials, especially lignin. The comparative yield percentage of all of the studied samples can be found in the Supporting Information (Table S1). Finally, bulky cellulose fibers were further treated with 1% H_2O_2 solution using an ultrasonic probe, and the slurry was dried to obtain the white-colored fibers (see Figure 1).

Hydrogen peroxide in AHP solution promotes delignification and dissolves hemicellulose by its oxidative action, resulting in almost pure cellulose fibers.[16] The effect of AHP solution on the delignification is sensitive to pH, and the solution is most effective at pH around 11.5−11.6.[17,33] Our results on yield percent of cellulose showed similar trends with other studies; however, the hemicellulose and lignin percentages varied. For example, Johar et al. reported that untreated rice husk consists of 35%, 33%, 23%, and 25% of cellulose, hemicellulose, lignin, and silica ash, respectively.[34] In general, the content and chemical composition of hemicellulose of plant biomass is influenced by plant varieties, growth conditions, and harvesting season.[35] In our study, a small portion of silica was detected in the rice husk sample after AHP hydrolysis; this might be due to part of the silica being bonded covalently with an organic compound.[11] It is expected that AHP hydrolysis coupled with an ultrasonic bath might be useful to extract the lignin and silica by disrupting the complex structure of lignocellulose. It is indicated that the applied methodology in the study could be an alternative and practical approach to the recovery of lignocellulosic components along with silica. Ultrasonication impacts the physical and chemical characteristics of the biomass, such as delignification, cellulose, and hemicellulose content, particle size, and surface area.[36]

Compositional Analysis. The lignocellulosic composition of the sample was analyzed by HPLC at each stage and presented in Table 1. Cellulose was estimated in glucan, and hemicellulose was calculated as the sum of xylan, galactan, arabinan, and manan. The concentrations of cellulose, hemicellulose, lignin, and silica in raw samples ranged from 31% to 40%, 19% to 22%, 23% to 35%, and 7% to 20%, respectively (see Table 1). Among the raw samples, the highest amount of cellulose was obtained from SB (39.7%), whereas cellulose from RH and PS was around 35.1% and 31.1%, respectively. The highest percent of lignin was obtained from raw-PS (35.1%).

After subsequent treatment, the cellulose concentration was drastically increased, whereas the concentrations of both hemicellulose and lignin were decreased. Since hemicellulose is an amorphous structure, it is easily dissolved by sulfuric acid treatment but keeps cellulose and lignin intact.[37] The plant biomass treated with diluted sulfuric acid can dissolve around 80% of hemicellulose.[38] In our study, hemicellulose (xylan) was removed in a similar range, which was between 79% and 91%. Besides, sulfuric acid also removed metal ions, chloride, and phosphate; removal of these impurities helps prevent contamination during the recovery process, and it can bring synergistic benefits in later stages of harvesting silica-based materials from agricultural biomass.[14,39]

AHP hydrolysis coupled with an ultrasonic bath dissolved lignin and silica. It also dissolved the remaining portion of hemicellulose. In this step, lignin concentration extracted around 54%, 64%, and 92% from PS, RH, and SB, respectively. As the yield percent of lignin was still high in PS and RH after AHP hydrolysis, this step was repeated, and it dissolved more than 90% of lignin from PS and RH of the initial lignin. The AHP pretreatment performed at 30 °C for 24 h in an incubator shaker removed 91.5% from corn stover.[40] Ultrasonication of cellulose pulp further decreased the remaining hemicellulose and lignin. For instance, xylan decreased from 10.1% to 1.4% during AHP hydrolysis coupled with an ultrasonic bath and an additional 0.9% reduction after irradiation with an ultrasonic probe. Overall, hemicellulose was decreased from 21.4% to

https://doi.org/10.1021/acssuschemeng.0c09342
ACS Sustainable Chem. Eng. XXXX, XXX, XXX−XXX

Table 2. Comparison of Different Pretreatment Methods Reported in the Literature[a]

biomass	pretreatment method	lignocellulosic contents and silica (%) cellulose	HC/lignin	silica	ref
PS	hydrothermal, high-pressure CO_2 at 190 °C	45.5	9.2/42.6	na	53
RH	NaOH 4 wt % for 2 h, acetic acid buffer, 10 M H_2SO_4, 50 °C for 40 min.	96.0	33.0/21.0	25.0	34
RH	NaOH 4 wt % for 3 h, acetate buffer for 4 h, 64% H_2SO_4, 50 °C for 40 min	73.8	19.2/1.6	na	54
RH	NaOH 5 wt %, 120 °C for 45 min, 25% acetic acid, 5% H_2O_2 and HNO_3 10 wt %, 120 °C for 2 h	65.5	8.9/15.9	na	55
SB	NaOH 5 wt %, 55 °C for 2 h, H_2O_2	80.5	15.45/6.5	na	56
SB	1 h ozonization, 2 h alkalinization and ultrasonication (5 min)	51.8	11.2/22.3	na	57
SB	Ultrasound-assisted titanium dioxide, 1% H_2O_2, 75 °C for 60 min, metal salt	94.0 holocellulose	78.7 delignification	na	48
PS	0.1 M H_2SO_4, 75 °C for 2 h, alkaline hydrogen peroxide, 50 °C for 2 h, ultrasonically assisted for 2 h, 1% H_2O_2	76.0	4.9/9.0	10.8	our study
RH		70.7	5.5/5.5	20.0	
SB		76.0	7.0/2.4	7.0	

[a]Abbreviations: PS, RH, and SB represent peanut shell, rice husk, and sugar cane bagasse, respectively. HC represents hemicellulose, and "na" indicates data is not available.

4.9% in PS. Similarly, the lignin concentration in raw SB was 30.4%, and after ultrasonication, it was found to be only 0.5%. However, around 5.5−9% lignin was observed in PS and RH cellulose even after ultrasonication (see Table 1). This shows that the pretreatment method applied in this study might not be equally effective for every sample due to the chemical compositions and structural differences. Further study is needed to verify the effects of the ultrasonic-assisted technique on the chemical, composition, and structural differences in detail.

The cellulose concentration in our study from SB was lower than those reported in other studies by Yu et al. (~43.6%) and Ingle et al. (~42.4%). This might be due to the differences in the extraction conditions, while the hemicellulose and lignin contents were similar to these studies.[41,42] In another study, the cellulose, hemicellulose, and lignin contents of SB bleached with H_2O_2 were 84.7%, 5.0%, and 2.7%, respectively,[43] and our findings are consistent with the reported values. Similarly, the PS composition (wt %) was 49%, 33%, 8%, and 9% for cellulose, lignin, hemicellulose, and ash.[44] The differences in the lignocellulosic compositions depend on various factors such as plant varieties, climatic conditions, geographical location, sample preparation, and methods of analysis, which might be the reasons for the variations in the chemical compositions in this study.[5] Nevertheless, the calculated values in our study were within the range reported by several research teams.[5,34,45,46]

Ultrasonic treatment of aqueous media produces cavitation, which generates a high temperature, pressure, and shear force.[47] These extreme conditions decompose water and H_2O_2 into many reactive oxygen species such as superoxide ions and hydroxyl radicals.[48] These radicals depolymerized the side chain of lignin and breakdown hydrogen ions of the hemicellulose backbone (xylan).[40] In our study, a transparent homogeneous slurry was produced after ultrasonication. However, due to its hydrophilic properties, a colloidal suspension aggregated as a cluster after a few hours of storage; images are available in the Supporting Information (Figure S2).[45,49] The solvent system and ultrasonic frequency might influence the magnitude of the ultrasonic effects.[50] Ultrasound treatment is also useful to disintegrate into nanocrystalline cellulose and decrease the optical haze of the suspension.[51] Csiszar et al. synthesized a transparent nanosized cellulose suspension from bleached cotton using a low-frequency ultrasound-assisted method and developed films from the suspension with improved barrier and mechanical properties.[52] Furthermore, the lignocellulose fractionation from different agricultural byproducts and their successful extraction conditions are compared in Table 2. In this study, a relatively simple process is applied for the fractionation of byproducts compared to the conventional method. Besides, it could enable the recovery of biopolymers effectively, so that this might be an alternative approach to convert agricultural byproducts into value-added materials.

Acid-Soluble Lignin Analysis. All of the samples including raw and AHP-treated (cellulose) PS, RH, and SB exhibited similar UV spectra absorption patterns characteristic of native lignin (see Figure 2). Obtained spectra suggested that

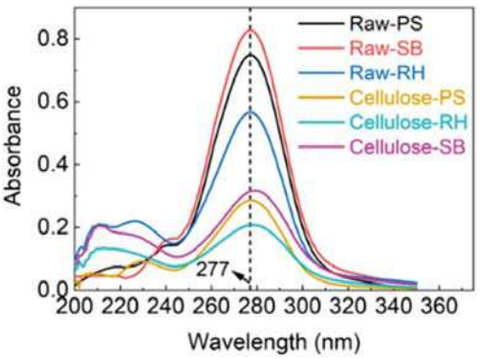

Figure 2. Ultraviolet spectra (UV) of Klason lignin (acid-soluble lignin) filtrates prepared from raw and alkaline peroxide-treated peanut shell (PS), rice husk (RH), and sugar cane bagasse (SB).

the acid-soluble lignin has two broad absorption spectra around 205 nm and a prominent peak at 277 nm. Characteristic absorption maxima near 280 nm are attributed primarily to the benzenoid moieties of lignin.[58] However, under acidic conditions, furfural and 5-hydroxymethyl-2 furfuraldehyde (HMF) could be produced from pentoses and hexoses, respectively.[59] Chi et al. also mentioned that furfural and HMF showed characteristic peaks around 277 and 285 nm, respectively. Thus, the broad peak around 277 nm might also be due to degraded carbohydrate and lignin interference. Nevertheless, the intensity of the absorption spectra around 277 nm is drastically decreased after AHP hydrolysis compared

https://doi.org/10.1021/acssuschemeng.0c09342
ACS Sustainable Chem. Eng. XXXX, XXX, XXX−XXX

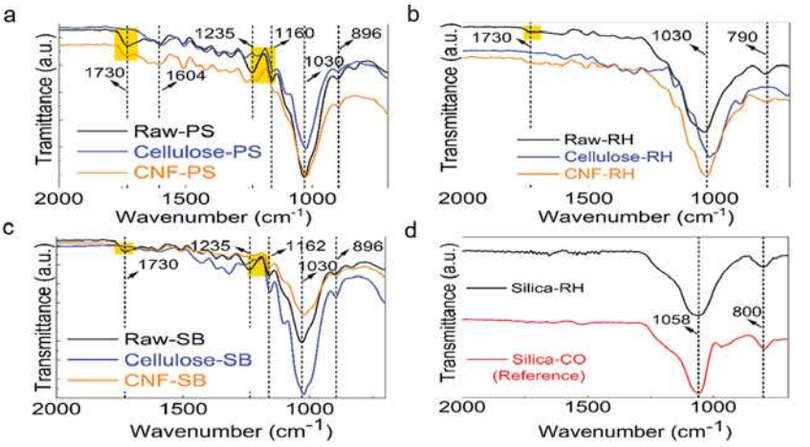

Figure 3. FTIR analysis of the cellulose fibers at each stage of treatment: (a) peanut shell (PS), (b) rice husk (RH), and (c) sugar cane bagasse (SB). (d) Representative silica spectrum recovered from rice husk compared to the spectrum from commercially available silica.

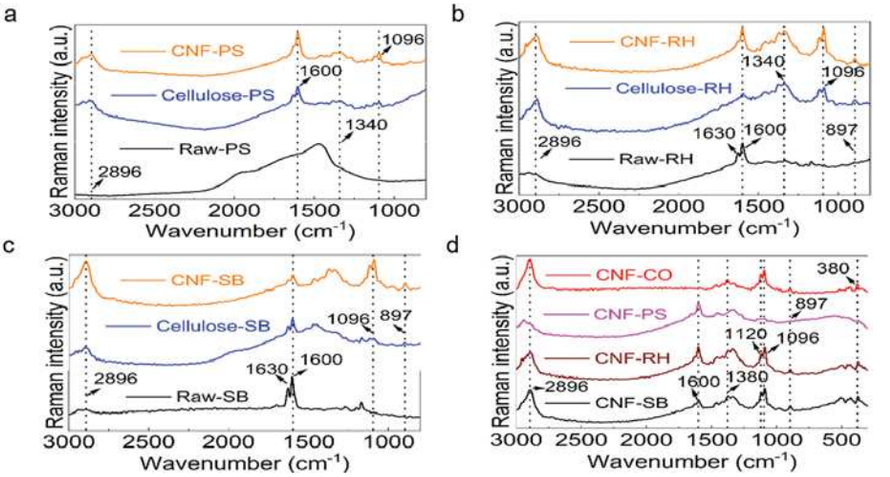

Figure 4. Raman analysis of the cellulose fibers at each stage of treatment: (a) peanut shell (PS), (b) rice husk (RH), and (c) sugar cane bagasse (SB). (d) Spectra of CNF from PS, RH, and SB compared to the spectrum from commercial cellulose nanofibers (CNF-CO).

to raw samples, indicating hemicellulose and lignin removal. These results supported the calculated value of hemicellulose and lignin during the process in which the concentration is decreased with AHP hydrolysis (see Table 1).

FTIR Analysis. Figure 3 shows the FTIR spectra recorded for raw, AHP-treated sample, and CNFs from each sample. The broad peak around 3300−3350 cm^{-1}, corresponding to OH stretching vibrations of cellulose, was obtained from each sample (Figure S3). The band between 1510 and 1605 cm^{-1} usually corresponds to the stretching structure of the aromatic groups of lignin.[47] The band at 1730 cm^{-1} was present in the FTIR spectra of fibers related to the C═O bonds of unconjugated ketones present in the hemicellulose.[46] The progressive reduction of these peaks in the samples indicated that the acid and AHP hydrolysis removed most noncellulosic components regardless of the samples. The intensity of the hemicellulose and lignin peaks was high in the raw samples, as presented in Figure 3 (see Figure 3a−c). The peak intensity decreased in the 1730 and 1236 cm^{-1} bands with AHP hydrolysis and finally almost disappeared after ultrasonic treatments. These results indicated removal of hemicellulose and lignin from the samples due to sulfuric acid hydrolysis, AHP hydrolysis, and H_2O_2 coupled with ultrasonication. The prominent bands around 1160 cm^{-1} in peanut shell and sugar cane bagasse fibers (see Figure 3a and 3c) and 1030 cm^{-1} observed in all of the samples refer to the C−H stretching vibration of C−O and the structure of the cellulose components.[60] No significant shifts and differences were observed in the spectra corresponding to raw, AHP-treated, and ultrasonically treated fibers. The obtained results indicated that the cellulose molecular structure remains unchanged during the process. The absorption band intensity at around 896 cm^{-1} is decreased as compared to the raw samples, and the band is assigned to C−O−C bridge stretching of the amorphous absorption band.[61] However, the band intensities were varied among the samples; this indicates that the applied method may not have a similar effect for the separation of the lignocellulosic components with the selected agricultural byproducts. In our previous study, we analyzed CNFs produced from sugar cane bagasse using a similar method with Raman spectroscopy. The results revealed that the applied method successfully removed noncellulosic components compared to raw SB.[22]

The FTIR pattern of silica nanoparticles from rice husks was like commercial silica (see Figure 3d). The major asymmetric stretching of Si−O−Si that occurred at around 1058 cm^{-1} is a characteristic peak of silica.[62] The intense band at around 800 cm^{-1} was assigned for symmetric stretching of Si−O−Si.[14] The

https://doi.org/10.1021/acssuschemeng.0c09342
ACS Sustainable Chem. Eng. XXXX, XXX, XXX−XXX

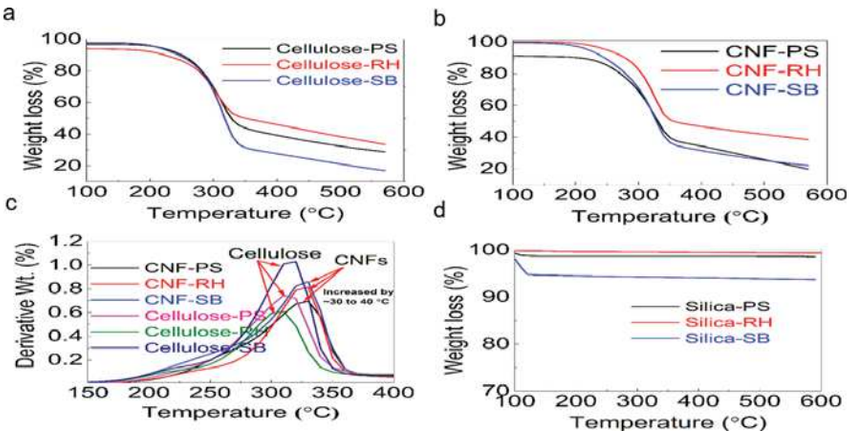

Figure 5. (a) TGA and (b) DTGA of the peanut shell (PS), rice husk (RH), and sugar cane bagasse (SB) at a different stage of treatment. (c) Comparison among the cellulose nanofibers (CNFs) of PS, RH, and SB.

FTIR spectrum of the recovered hemicellulose from SB (representative sample) can be found in Supporting Information Figure S4. The bands around 2913 and 2827 cm^{-1} might be due to C−H stretching vibrations in hemicellulose. Yao et al. reported the bands around 2920 and 2877 cm^{-1} in hemicellulose extracted by hot water from SB.[63] In another similar study, the absorption bands of native hemicellulose (industrial xylan-rich hemicellulose) were reported around 2919, 1635, 1376, 1242, 1060, and 898 cm^{-1}.[35] However, in our study, the FTIR peaks were at different wavenumbers, but the spectral trend was similar to the peaks mentioned above. The absorption peaks may be due to the structural difference of our hemicellulose.

Raman Analysis. Figure 4 shows the comparative Raman spectra of the samples in each treatment stage and compares CNF derived from each sample with the commercial CNF. Prominent peaks were observed in all CNF samples at 2896 and 1340 cm^{-1} assigned to CH and CH_2 stretching, 1096 cm^{-1} assigned to CC and CO stretching, 897 cm^{-1} assigned to CH, and 380 cm^{-1} assigned to cellulose stretching and ring deformation.[64] These peaks were more intense compared to the cellulose samples. The observed peaks for cellulose in our study are in agreement with the previously reported peaks from lignocellulosic biomass.[64−66] The dominant peaks for lignin in the lignocellulosic samples were suggested at around 1600 and 1632 cm^{-1} assigned to C═C stretching and lignin skeletal vibration.[67−69] The sharp peaks were recorded at around 1600 and 1630 cm^{-1} from all raw samples, and eventually, the intensity of the peaks was drastically decreased after subsequent treatment. These results strongly indicate that the lignin was successfully removed from the samples by the method used in our study. On the contrary, in CNF-PS, the peaks around 1600 cm^{-1} were also absorbed, indicating the presence of lignin residue even after ultrasonication. These findings supported the HPLC results in which the highest percentage of lignin was determined in CNF-PS. Similarly, the broad peak around 1450 cm^{-1} in raw-PS is unique compared with other raw samples and can be associated with undigested proteins in the PS cell wall and other naturally occurring fluorescent molecules found in PS. Ultrasound-treated samples (i.e., CNF) followed a similar pattern with commercial cellulose nanofiber (CNF-CO); the results indicate the effectiveness of the methodology used.

Thermal Analysis. The thermogravimetric analysis (TGA) and derivative of thermogravimetric analysis (DTGA) curves of the samples are shown in Figure 5. During the thermal analysis, a sample undergoes various degradation stages, including dehydration, depolymerization, decomposition, and subsequent oxidation, leading to a charred residue. The four stages of decomposition weight loss have been observed. In the first stage, decomposition occurred at a temperature below 120 °C, giving almost 9% weight loss in ultrasonically isolated nanocellulose from PS (CNF-PS). This result corresponds to the drying period, where light volatile compounds and water are liberated throughout the procedure. In the second stage, hemicellulose degradation (200−300 °C) induced around 17−29% weight loss. In the third (250−350 °C) and fourth stages (200−500 °C), cellulose and lignin degradation occurred. The TGA curves and corresponding weight loss values with increased temperature showed that the maximum weight loss (around 50−60%) occurred in the range of 250−350 °C regardless of the samples (see Figure 5a and 5b and Table S2). Interestingly, the degradation temperature of the samples showed that cellulose nanofibers from rice husk (CNF-RH) exhibited a higher decomposition temperature than CNF-PS and CNF-SB. However, CNFs from PS and SB exhibited similar decomposition temperatures (see Figure 5b).

The maximum degradation temperature was determined from the DTGA curves. Figure 5c presents the comparative degradation pattern of cellulose treated with AHP (cellulose fibers), and ultrasonicated samples (CNFs) were different in terms of the shape of the curves and degradation temperature. The AHP-treated sample curves have two prominent peaks from the hemicellulose degradation in the temperature range 200−300 °C and another shoulder in the temperature range 250−350 °C, which corresponds to cellulose. There were no distinct peaks observed above 400 °C; this may be due to the decomposition of the lignocellulosic components. The decomposition temperature is increased in ultrasonically treated samples by around 30−40 °C compared to AHP-treated samples. The peaks from the ultrasonically treated samples are relatively less broad than AHP-treated samples (see Figure 5c); this may be due to removing noncellulosic components after ultrasonication. Ultrasound irradiation disrupts the amorphous cellulose region and removes the remaining hemicellulose and lignin, thus increasing the thermal stability. The observed results demonstrated that the applied

https://doi.org/10.1021/acssuschemeng.0c09342
ACS Sustainable Chem. Eng. XXXX, XXX, XXX−XXX

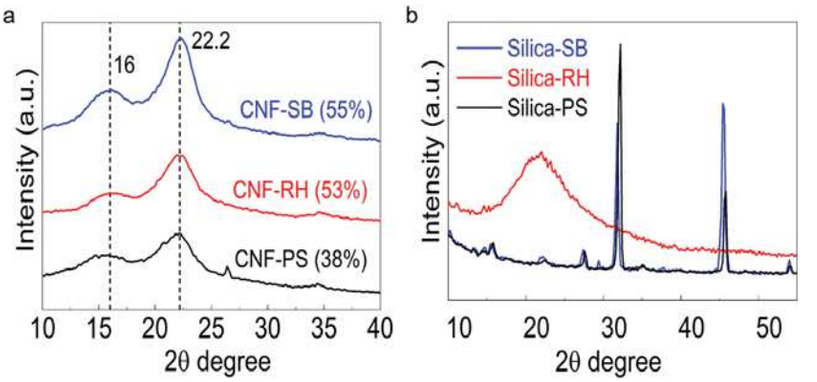

Figure 6. XRD pattern and crystallinity of (a) cellulose nanofiber (CNF) and (b) silica nanoparticles (SNPs) from peanut shell (PS), rice husk (RH), and sugar cane bagasse (SB).

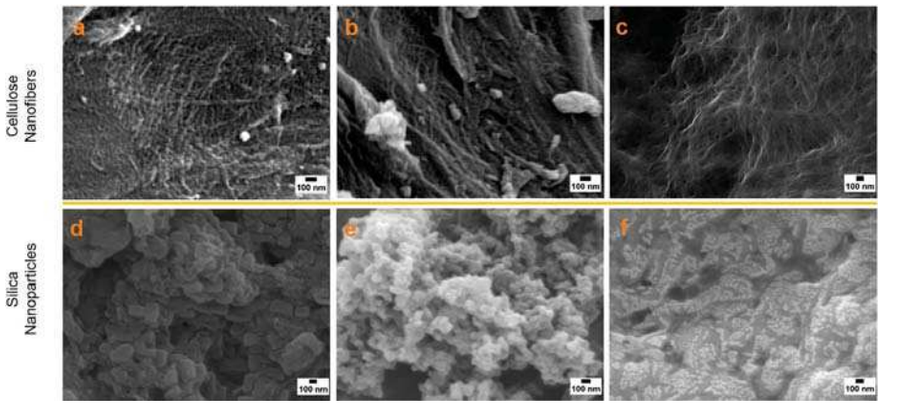

Figure 7. FE-SEM images of cellulose nanofibers (top): (a) peanut shell (PS), (b) rice husk (RH), and (c) sugar cane bagasse (SB). Silica nanoparticles (bottom): (d) PS, (e) RH, and (f) SB.

procedure increased the decomposition temperature of isolated cellulose nanofibers. Thus, the obtained cellulose nanofibers may be a potential nanofiller in composite materials to enhance the thermal property.

In addition, the residue amount left was around 20−40%. RH cellulose was remarkably high (~40%) among the samples obtained from AHP and ultrasonically treated samples; similar values have been reported in the literature on rice husk.[34] It may be due to the more crystalline cellulose or some silica portion remaining on the samples even after AHP and ultrasonic treatment. Around 2% (mass) of silica was detected in this study from qualitative analysis of the EDS data obtained from CNF-RH. The linear thermogram indicates the outstanding thermal stability of silica up to 600 °C from all samples (see Figure 5d). The weight loss of around 1−5% from 100 to 120 °C is associated with the desorption of water.

X-ray Analysis. Comparative analysis of the XRD pattern and crystallinity percentage of the cellulose nanofibers by XRD measurement is given in Figure 6a. All of the XRD patterns showed three prominent defined diffraction peaks at 2θ = 16.5°, 22°, and 35°. These are the characteristics peaks of cellulose.[70,71] The order of crystallinity index (CrI) among the samples was in the order SB > RH > PS with a sharp peak around 22° for all samples. The XRD pattern was also compared to commercial cellulose nanocrystals (CNCs) and cellulose nanofibers (CNFs) (Figure S5). The XRD spectra for all samples studied followed a similar pattern with commercial cellulose; the highest crystallinity percentage was obtained from commercial CNCs (Figure S5). The sugar cane bagasse-derived CNFs crystallinity percentage (54.8%) was identical to that of commercial CNFs (55.9%). The crystallinity percentage of the study samples was consistent with the reported data. For example, CrI was 58% in sugar cane bagasse-derived nanocellulose using continuous steam explosion combined with ultrasonication.[72] In another study, CrI was 59% in rice husks-derived nanocellulose using sulfuric acid hydrolysis.[34] Similarly, the CrI of nanocellulose from peanut shells was 65% isolated using acidified sodium chlorite and subsequently went through a high-pressure homogenizer.[44] However, the percent crystallinity of nanocellulose may vary based on the measurement methods and isolation techniques.[73] The increase in the crystallinity of cellulose is expected to increase their stiffness and strength. Thus, it was assumed to improve the mechanical properties and reinforcement capabilities. The XRD results supported the assumption that ultrasonic-assisted chemical methods could successfully isolate semicrystalline cellulose nanofibers from selected agricultural byproducts.

In addition to cellulose nanofibers, silica nanoparticles (SNPs) were also characterized by XRD (see Figure 6b). Silica nanoparticles from RH showed broad diffused peaks with maximum intensity at 2θ = 22°, indicating the amorphous nature of silica. Amorphous silica was reported from acid-treated RH and pyrolyzed at 700 °C.[5,39,74] The SiO_2 in rice husk ash formed by combustion below 800 °C was found to be amorphous.[75] However, crystallization of silica starts to occur at a higher temperature at or above 900 °C.[76] Interestingly, the XRD pattern of silica obtained from PS and SB was crystalline despite the same pyrolysis conditions. The XRD results were

https://doi.org/10.1021/acssuschemeng.0c09342
ACS Sustainable Chem. Eng. XXXX, XXX, XXX−XXX

further corroborated and confirmed by SEM image analysis and discussed in the following section.

Surface Morphology. The surface morphology of the cellulose nanofibers (CNFs) was investigated using FE-SEM (Figure 7). The CNFs from three different samples have different shapes and orientations (see Figure 7a−c). The ultrasonic irradiation surfaces of the CNFs derived from PS, RH, and SB were web-like, parallel, and tangled, respectively. The diameter of the CNFs differed in different samples; the fiber diameter was <100 nm. In particular, the CNFs diameter was varied among the samples, which ranged from 2 to 12 nm, 20 to 80 nm, and 20 to 70 nm in PS, RH, and SB, respectively; evaluation of the fiber diameter can be found in the Supporting Information (Figure S6a−c).

The SEM images of SNPs from AHP-treated samples followed by pyrolysis are presented in Figure 7d−f. The diameter of the SNPs was also evaluated, and grain sizes were different among the samples, in which the SNPs sizes ranged from 100 to 350 nm, 40 to 130 nm, and 10 to 70 nm in PS, RH, and SB, respectively (Figure S6d−f). The shape of the SNPs was different among the studied samples in which RH-derived SNPs exhibited a coral sponge-like appearance comprised of fused agglomerates of spherical structure.[77] It could be seen that particles are spherical, and some of the particles were agglomerated in PS-derived SNPs (see Figure 7f). In conjunction, the structure of the SNPs synthesized from SB also showed a well-defined round structure formed with scattered pores.[78] The obtained SNPs structures in our study were a typical form of mesoporous materials. These data were further supported by BET analysis as discussed in the following section. Furthermore, the silica content in the samples was confirmed by EDS (Figure S7), and the amount of silica was qualitatively determined and around 70−80%. The highest weight percentage of silica was obtained from RH. In addition, more SEM images of both CNF and SNPs from all samples at different magnifications are also found in the Supporting Information (Figure S8).

BET Analysis. The BET surface area, average pore radius, and pore volume of silica from each sample were compared in this study, and the results are presented in Table 3. In particular, the surface area showed similar results for silica obtained from PS and SB, which were 3.9 and 2.5 m^2/g with total pore volumes of 0.01 and 0.02 cc/g, respectively. However, these values are high in silica from RH (37.5 m^2/g and 0.08 cc/g). The specific surface area values obtained by the BET method were relatively smaller in this study than the reported method from agricultural biomass.[77−80] However, the obtained pore radius and pore volume were in a similar range to that reported in the literature. The observed smaller surface area could be ash impurity in the silica because the samples were directly analyzed without purification. These findings showed that the conversion of agricultural byproducts to biogenic silica (a precursor to mesoporous silica) is attractive from both an economic and an environmental perspective, suggesting that this could be considered for further research.

Table 3. BET Analysis of the Silica Nanoparticles Obtained from PS, RH, and SB

parameter	silica-PS	silica-RH	silica-SB
pore radius (nm)	1.5	1.4	1.3
pore volume (cc/g)	0.01	0.08	0.02
BET surface area (m^2/g)	3.9	37.5	2.5

CONCLUSIONS

In this study, biopolymers and silica from agricultural byproducts such as sugar cane bagasse (SB), peanut shell (PS), and rice husk (RH) were fractionated in an integrated system using an ultrasonic-assisted chemical method. The employed process was feasible to fractionate and recover cellulose, hemicellulose, lignin, and silica from the raw materials. The characterization data indicated that the CNFs from SB were more crystalline than the CNFs from PS and RH. The silica nanoparticles (SNPs) from SB and PS were crystalline, but SNPs from RH were amorphous. However, the shape and size of the CNFs and SNPs from each sample varied, indicating the different structural properties based on the source materials. For instance, the CNFs were web-like, parallel, and entangle from the surface structures. The SNPs had a mesoporous structure which were spherical, sponge-like, and well-defined round shapes in PS, RH, and SB, respectively. Regardless of the samples, the thermal decomposition temperature of the CNFs was increased compared to that of cellulose fibers. Therefore, the described method could be considered as a potential approach for the comprehensive use of agricultural byproducts in a sustainable biopolymer application.

ASSOCIATED CONTENT

Supporting Information

The Supporting Information is available free of charge at https://pubs.acs.org/doi/10.1021/acssuschemeng.0c09342.

Biopolymer sequential fractionation process; recovery of isolated cellulose, hemicellulose, lignin, and silica in weight percentage; ultrasonicated CNFs and agglomerated CNFs; FTIR spectra of PS, RH, and SC at different treatment stages; FTIR spectra of recovered hemicellulose from sugar cane bagasse; percentage of weight loss at different temperatures during thermal analysis; comparative XRD spectra of cellulose nanofibers from peanut shell, rice husk, sugar cane bagasse, commercial cellulose nanofiber, and cellulose nanocrystal; cellulose nanofiber diameter and silica nanoparticles diameter, SNPs from peanut shell, SNPs from rice husk, and SNPs from sugar cane bagasse; energy-dispersive spectra of silica from agricultural byproducts from PS, RH, and SB; FE-SEM images of cellulose nanofibers and silica nanoparticles (PDF)

AUTHOR INFORMATION

Corresponding Authors

Byungjin Min − *Department of Food and Nutritional Sciences, Tuskegee University, Tuskegee, Alabama 36088, United States*; Phone: 334-727-8393; Email: bmin@tuskegee.edu

Vijaya K. Rangari − *Department of Materials Science and Engineering, Tuskegee University, Tuskegee, Alabama 36088, United States*; orcid.org/0000-0002-3962-1686; Phone: 334-724-4875; Email: vrangari@tuskegee.edu

Authors

Naresh Shahi − *Integrative Biosciences Ph.D. Program, Tuskegee University, Tuskegee, Alabama 36088, United States*; orcid.org/0000-0002-6666-805X

https://doi.org/10.1021/acssuschemeng.0c09342
ACS Sustainable Chem. Eng. XXXX, XXX, XXX−XXX

Pixiang Wang − *Center for Bioenergy and Bioproducts, Auburn University, Auburn, Alabama 36849, United States;* orcid.org/0000-0002-3373-4006

Sushil Adhikari − *Center for Bioenergy and Bioproducts, Auburn University, Auburn, Alabama 36849, United States;* orcid.org/0000-0002-6539-6822

Complete contact information is available at: https://pubs.acs.org/10.1021/acssuschemeng.0c09342

Notes

The authors declare no competing financial interest.

■ ACKNOWLEDGMENTS

This research was supported by the grant awarded from the United States Department of Agriculture (USDA)/National Institute of Food and Agriculture (NIFA), grant no. 2015-38821-24376. The authors also acknowledge the financial support of NSF-RISE no. 1459007, NSF-CREST no. 1735971, and NSF-MRI-1531934 grants.

■ REFERENCES

(1) Chen, M. J.; Shi, Q. S. Transforming Sugarcane Bagasse into Bioplastics via Homogeneous Modification with Phthalic Anhydride in Ionic Liquid. *ACS Sustainable Chem. Eng.* **2015**, *3* (10), 2510−2515.

(2) Barhoum, A.; Jeevanandam, J.; Rastogi, A.; Samyn, P.; Boluk, Y.; Dufresne, A.; Danquah, M. K.; Bechelany, M. Plant Celluloses, Hemicelluloses, Lignins, and Volatile Oils for the Synthesis of Nanoparticles and Nanostructured Materials. *Nanoscale* **2020**, *12* (45), 22845−22890.

(3) Zhu, P.; Abdelaziz, O. Y.; Hulteberg, C. P.; Riisager, A. New Synthetic Approaches to Biofuels from Lignocellulosic Biomass. *Curr. Opin. Green Sustain. Chem.* **2020**, *21*, 16−21.

(4) Alokika; Anu; Kumar, A.; Kumar, V.; Singh, B. Cellulosic and Hemicellulosic Fractions of Sugarcane Bagasse: Potential, Challenges and Future Perspective. *Int. J. Biol. Macromol.* **2021**, *169*, 564−582.

(5) Chen, H.; Wang, W.; Martin, J. C.; Oliphant, A. J.; Doerr, P. A.; Xu, J. F.; DeBorn, K. M.; Chen, C.; Sun, L. Extraction of Lignocellulose and Synthesis of Porous Silica Nanoparticles from Rice Husks: A Comprehensive Utilization of Rice Husk Biomass. *ACS Sustainable Chem. Eng.* **2013**, *1* (2), 254−259.

(6) Salas, C.; Nypelö, T.; Rodriguez-Abreu, C.; Carrillo, C.; Rojas, O. J. Nanocellulose Properties and Applications in Colloids and Interfaces. *Curr. Opin. Colloid Interface Sci.* **2014**, *19* (5), 383−396.

(7) Pachuau, L. Application of Nanocellulose for Controlled Drug Delivery. In *Nanocellulose and Nanohydrogel Matrices: Biotechnological and Biomedical Applications*; Mohammad, J., Faruq, M., Eds.; Wiley-VCH Verlag GmbH & Co. KGaA., 2017; pp 1−19.

(8) Ajao, O.; Marinova, M.; Savadogo, O.; Paris, J. Hemicellulose Based Integrated Forest Biorefineries: Implementation Strategies. *Ind. Crops Prod.* **2018**, *126* (July), 250−260.

(9) Sun, X. F.; Wang, H. H.; Jing, Z. X.; Mohanathas, R. Hemicellulose-Based PH-Sensitive and Biodegradable Hydrogel for Controlled Drug Delivery. *Carbohydr. Polym.* **2013**, *92* (2), 1357−1366.

(10) Farhat, W.; Venditti, R.; Quick, A.; Taha, M.; Mignard, N.; Becquart, F.; Ayoub, A. Hemicellulose Extraction and Characterization for Applications in Paper Coatings and Adhesives. *Ind. Crops Prod.* **2017**, *107*, 370−377.

(11) Upton, B. M.; Kasko, A. M. Strategies for the Conversion of Lignin to High-Value Polymeric Materials: Review and Perspective. *Chem. Rev.* **2016**, *116* (4), 2275−2306.

(12) Lazaro, A.; Vilanova, N.; Barreto Torres, L. D.; Resoort, G.; Voets, I. K.; Brouwers, H. J. H. Synthesis, Polymerization, and Assembly of Nanosilica Particles below the Isoelectric Point. *Langmuir* **2017**, *33* (51), 14618−14626.

(13) Rovani, S.; Santos, J. J.; Corio, P.; Fungaro, D. A. Highly Pure Silica Nanoparticles with High Adsorption Capacity Obtained from Sugarcane Waste Ash. *ACS Omega* **2018**, *3* (3), 2618−2627.

(14) Vaibhav, V.; Vijayalakshmi, U.; Roopan, S. M. Agricultural Waste as a Source for the Production of Silica Nanoparticles. *Spectrochim. Acta, Part A* **2015**, *139*, 515−520.

(15) Kauldhar, B. S.; Sooch, B. S.; Rai, S. K.; Kumar, V.; Yadav, S. K. Recovery of Nanosized Silica and Lignin from Sugarcane Bagasse Waste and Their Engineering in Fabrication of Composite Membrane for Water Purification. *Environ. Sci. Pollut. Res.* **2021**, *28*, 7491.

(16) Ho, M. C.; Ong, V. Z.; Wu, T. Y. Potential Use of Alkaline Hydrogen Peroxide in Lignocellulosic Biomass Pretreatment and Valorization - A Review. *Renewable Sustainable Energy Rev.* **2019**, *112* (May), 75−86.

(17) Su, Y.; Du, R.; Guo, H.; Cao, M.; Wu, Q.; Su, R.; Qi, W.; He, Z. Fractional Pretreatment of Lignocellulose by Alkaline Hydrogen Peroxide: Characterization of Its Major Components. *Food Bioprod. Process.* **2015**, *94*, 322−330.

(18) Mittal, A.; Katahira, R.; Donohoe, B. S.; Black, B. A.; Pattathil, S.; Stringer, J. M.; Beckham, G. T. Alkaline Peroxide Delignification of Corn Stover. *ACS Sustainable Chem. Eng.* **2017**, *5* (7), 6310−6321.

(19) Alvarez-Vasco, C.; Zhang, X. Alkaline Hydrogen Peroxide Pretreatment of Softwood: Hemicellulose Degradation Pathways. *Bioresour. Technol.* **2013**, *150*, 321−327.

(20) Abd-Talib, N.; Mohd-Setapar, S. H.; Asli, U. A.; Pa'ee, K. F.; Len, K. Y. T.; Mohd-Nasir, H. Silica Removal by Alkaline Hydrogen Peroxide Treatment to Enhance the Conversion of Rice Straw to Sugars. *Mater. Today Proc.* **2020**, *31* (xxxx), 145−149.

(21) Dutra, E. D.; Santos, F. A.; Alencar, B. R. A.; Reis, A. L. S.; de Souza, R. d. F. R.; Aquino, K. A. d. S.; Morais Jr, M. A.; Menezes, R. S. C. Alkaline Hydrogen Peroxide Pretreatment of Lignocellulosic Biomass: Status and Perspectives. *Biomass Convers. Biorefin.* **2018**, *8* (1), 225−234.

(22) Shahi, N.; Min, B.; Sapkota, B.; Rangari, V. K. Eco-Friendly Cellulose Nanofiber Extraction from Sugarcane Bagasse and Film Fabrication. *Sustainability* **2020**, *12*, 6015.

(23) Shahi, N.; Joshi, G.; Min, B. Effect of Regenerated Cellulose Fibers Derived from Black Oat on Functional Properties of PVA-Based Biocomposite Film. *Processes* **2020**, *8* (9), 1149.

(24) Vidal, B. C.; Dien, B. S.; Ting, K. C.; Singh, V. Influence of Feedstock Particle Size on Lignocellulose Conversion - A Review. *Appl. Biochem. Biotechnol.* **2011**, *164* (8), 1405−1421.

(25) Yang, Y.; Ji, G.; Xiao, W.; Han, L. Changes to the Physicochemical Characteristics of Wheat Straw by Mechanical Ultrafine Grinding. *Cellulose* **2014**, *21* (5), 3257−3268.

(26) Ji, G.; Gao, C.; Xiao, W.; Han, L. Mechanical Fragmentation of Corncob at Different Plant Scales: Impact and Mechanism on Microstructure Features and Enzymatic Hydrolysis. *Bioresour. Technol.* **2016**, *205*, 159−165.

(27) Zhai, Q.; Li, F.; Wang, F.; Feng, J.; Jiang, J.; Xu, J. Ultrafine Grinding of Poplar Biomass: Effect of Particle Morphology on the Liquefaction of Biomass for Methyl Glycosides and Phenolics. *Cellulose* **2019**, *26* (6), 3685−3701.

(28) Baruah, J.; Nath, B. K.; Sharma, R.; Kumar, S.; Deka, R. C.; Baruah, D. C.; Kalita, E. Recent Trends in the Pretreatment of Lignocellulosic Biomass for Value-Added Products. *Front. Energy Res.* **2018**, *6* (DEC), 1−19.

(29) Sluiter, A.; Hames, B.; Ruiz, R.; Scarlata, C.; Sluiter, J.; Templeton, D.; Crocker, D. Determination of Structural Carbohydrates and Lignin in Biomass. *NREL/TP-510-42618*; NREL, Laboratory Analytical Procedure (LAP), 2012.

(30) Sluiter, A.; Hames, B.; Ruiz, R.; Scarlata, C.; Sluiter, J.; Templeton, D. Determination of Ash in Biomass. *NREL/TP-510-42622*; NREL, Laboratory Analytical Procedure (LAP), 2008.

(31) Wang, P.; Peng, H.; Adhikari, S.; Higgins, B.; Roy, P.; Dai, W.; Shi, X. Enhancement of Biogas Production from Wastewater Sludge via Anaerobic Digestion Assisted with Biochar Amendment. *Bioresour. Technol.* **2020**, *309* (April), 123368.

(32) Barana, D.; Salanti, A.; Orlandi, M.; Ali, D. S.; Zoia, L. Biorefinery Process for the Simultaneous Recovery of Lignin, Hemicelluloses, Cellulose Nanocrystals and Silica from Rice Husk and Arundo Donax. *Ind. Crops Prod.* **2016**, *86*, 31−39.
(33) Gould, J. M. Studies on the Mechanism of Alkaline Peroxide Delignification of Agricultural Residues. *Biotechnol. Bioeng.* **1985**, *27* (3), 225−231.
(34) Johar, N.; Ahmad, I.; Dufresne, A. Extraction, Preparation and Characterization of Cellulose Fibres and Nanocrystals from Rice Husk. *Ind. Crops Prod.* **2012**, *37* (1), 93−99.
(35) Zhu, R.; Liu, X.; Li, L.; Wang, Q.; Zhao, Q.; Liu, S.; Feng, W.; Xu, F.; Zhang, X. Valorization of Industrial Xylan-Rich Hemicelluloses into Water-Soluble Derivatives by in-Situ Acetylation in EmimAc Ionic Liquid. *Int. J. Biol. Macromol.* **2020**, *163*, 457−463.
(36) Bundhoo, Z. M. A.; Mohee, R. Ultrasound-Assisted Biological Conversion of Biomass and Waste Materials to Biofuels: A Review. *Ultrason. Sonochem.* **2018**, *40*, 298−313.
(37) Mäki-Arvela, P.; Salmi, T.; Holmbom, B.; Willför, S.; Murzin, D. Y. Synthesis of Sugars by Hydrolysis of Hemicelluloses- A Review. *Chem. Rev.* **2011**, *111* (9), 5638−5666.
(38) Yu, J. Microbial Production of Bioplastics from Renewable Resources. *In Bioprocessing for Value-Added Products from Renewable Resources* **2007**, 585−610.
(39) Wang, W.; Martin, J. C.; Fan, X.; Han, A.; Luo, Z.; Sun, L. Silica Nanoparticles and Frameworks from Rice Husk Biomass. *ACS Appl. Mater. Interfaces* **2012**, *4* (2), 977−981.
(40) Li, J.; Lu, M.; Guo, X.; Zhang, H.; Li, Y.; Han, L. Insights into the Improvement of Alkaline Hydrogen Peroxide (AHP) Pretreatment on the Enzymatic Hydrolysis of Corn Stover: Chemical and Microstructural Analyses. *Bioresour. Technol.* **2018**, *265* (May), 1−7.
(41) Yu, H.; You, Y.; Lei, F.; Liu, Z.; Zhang, W.; Jiang, J. Comparative Study of Alkaline Hydrogen Peroxide and Organosolv Pretreatments of Sugarcane Bagasse to Improve the Overall Sugar Yield. *Bioresour. Technol.* **2015**, *187*, 161−166.
(42) Ingle, A. P.; Philippini, R. R.; Silvério da Silva, S. Pretreatment of Sugarcane Bagasse Using Two Different Acid-Functionalized Magnetic Nanoparticles: A Novel Approach for High Sugar Recovery. *Renewable Energy* **2020**, *150*, 957−964.
(43) Oliveira, F. B. d.; Bras, J.; Pimenta, M. T. B.; Curvelo, A. A. d. S.; Belgacem, M. N. Production of Cellulose Nanocrystals from Sugarcane Bagasse Fibers and Pith. *Ind. Crops Prod.* **2016**, *93*, 48−57.
(44) Wang, B.; Li, D. Strong and Optically Transparent Biocomposites Reinforced with Cellulose Nanofibers Isolated from Peanut Shell. *Composites, Part A* **2015**, *79*, 1−7.
(45) Santucci, B. S.; Bras, J.; Belgacem, M. N.; Curvelo, A. A. d. S.; Pimenta, M. T. B. Evaluation of the Effects of Chemical Composition and Refining Treatments on the Properties of Nanofibrillated Cellulose Films from Sugarcane Bagasse. *Ind. Crops Prod.* **2016**, *91*, 238−248.
(46) Kumar, A.; Singh Negi, Y.; Choudhary, V.; Kant Bhardwaj, N. Characterization of Cellulose Nanocrystals Produced by Acid-Hydrolysis from Sugarcane Bagasse as Agro-Waste. *J. Mater. Phys. Chem.* **2014**, *2* (1), 1−8.
(47) Subhedar, P. B.; Gogate, P. R. Alkaline and Ultrasound Assisted Alkaline Pretreatment for Intensification of Delignification Process from Sustainable Raw-Material. *Ultrason. Sonochem.* **2014**, *21* (1), 216−225.
(48) Ramadoss, G.; Muthukumar, K. Mechanistic Study on Ultrasound Assisted Pretreatment of Sugarcane Bagasse Using Metal Salt with Hydrogen Peroxide for Bioethanol Production. *Ultrason. Sonochem.* **2016**, *28*, 207−217.
(49) Salas, C.; Nypelö, T.; Rodriguez-Abreu, C.; Carrillo, C.; Rojas, O. J. Nanocellulose Properties and Applications in Colloids and Interfaces. *Curr. Opin. Colloid Interface Sci.* **2014**, *19* (5), 383−396.
(50) Bussemaker, M. J.; Zhang, D. Effect of Ultrasound on Lignocellulosic Biomass as a Pretreatment for Biorefinery and Biofuel Applications. *Ind. Eng. Chem. Res.* **2013**, *52* (10), 3563−3580.
(51) Guo, J.; Guo, X.; Wang, S.; Yin, Y. Effects of Ultrasonic Treatment during Acid Hydrolysis on the Yield, Particle Size and Structure of Cellulose Nanocrystals. *Carbohydr. Polym.* **2016**, *135*, 248−255.
(52) Csiszar, E.; Kalic, P.; Kobol, A.; Ferreira, E. D. P. The Effect of Low Frequency Ultrasound on the Production and Properties of Nanocrystalline Cellulose Suspensions and Films. *Ultrason. Sonochem.* **2016**, *31*, 473−480.
(53) Ge, S.; Wu, Y.; Peng, W.; Xia, C.; Mei, C.; Cai, L.; Shi, S. Q.; Sonne, C.; Lam, S. S.; Tsang, Y. F. High-Pressure CO2 Hydrothermal Pretreatment of Peanut Shells for Enzymatic Hydrolysis Conversion into Glucose. *Chem. Eng. J.* **2020**, *385*, 123949.
(54) Collazo-Bigliardi, S.; Ortega-Toro, R.; Chiralt Boix, A. Isolation and Characterisation of Microcrystalline Cellulose and Cellulose Nanocrystals from Coffee Husk and Comparative Study with Rice Husk. *Carbohydr. Polym.* **2018**, *191* (March), 205−215.
(55) Hafid, H. S.; Omar, F. N.; Zhu, J.; Wakisaka, M. Enhanced Crystallinity and Thermal Properties of Cellulose from Rice Husk Using Acid Hydrolysis Treatment. *Carbohydr. Polym.* **2021**, *260*, 117789.
(56) Laluce, C.; Roldan, I. U.; Pecoraro, E.; Igbojionu, L. I.; Ribeiro, C. A. Effects of Pretreatment Applied to Sugarcane Bagasse on Composition and Morphology of Cellulosic Fractions. *Biomass Bioenergy* **2019**, *126* (March), 231−238.
(57) Perrone, O. M.; Colombari, F. M.; Rossi, J. S.; Moretti, M. M. S.; Bordignon, S. E.; Nunes, C. d. C. C.; Gomes, E.; Boscolo, M.; Da-Silva, R. Ozonolysis Combined with Ultrasound as a Pretreatment of Sugarcane Bagasse: Effect on the Enzymatic Saccharification and the Physical and Chemical Characteristics of the Substrate. *Bioresour. Technol.* **2016**, *218*, 69−76.
(58) Maekawa, E.; Ichizawa, T.; Koshijima, T. An Evaluation of the Acid-Soluble Lignin Determination in Analyses of Lignin by the Sulfuric Acid Method. *J. Wood Chem. Technol.* **1989**, *9* (4), 549−567.
(59) Chi, C.; Zhang, Z.; Chang, H. M.; Jameel, H. Determination of Furfural and Hydroxymethylfurfural Formed from Biomass under Acidic Conditions. *J. Wood Chem. Technol.* **2009**, *29* (4), 265−276.
(60) Šimkovic, I.; Kelnar, I.; Mendichi, R.; Bertok, T.; Filip, J. Composite Films Prepared from Agricultural By-Products. *Carbohydr. Polym.* **2017**, *156*, 77−85.
(61) Phinichka, N.; Kaenthong, S. Regenerated Cellulose from High Alpha Cellulose Pulp of Steam-Exploded Sugarcane Bagasse. *J. Mater. Res. Technol.* **2018**, *7* (1), 55−65.
(62) Kauldhar, B. S.; Yadav, S. K. Turning Waste to Wealth: A Direct Process for Recovery of Nano-Silica and Lignin from Paddy Straw Agro-Waste. *J. Cleaner Prod.* **2018**, *194*, 158−166.
(63) Yao, S.; Nie, S.; Zhu, H.; Wang, S.; Song, X.; Qin, C. Extraction of Hemicellulose by Hot Water to Reduce Adsorbable Organic Halogen Formation in Chlorine Dioxide Bleaching of Bagasse Pulp. *Ind. Crops Prod.* **2017**, *96*, 178−185.
(64) Lupoi, J. S.; Gjersing, E.; Davis, M. F. Evaluating Lignocellulosic Biomass, Its Derivatives, and Downstream Products with Raman Spectroscopy. *Front. Bioeng. Biotechnol.* **2015**, *3* (APR), 1−18.
(65) Agarwal, U. P. Raman Spectroscopy in the Analysis of Cellulose Nanomaterials. *ACS Symp. Ser.* **2017**, *1251*, 75−90.
(66) Alves, A. P. P.; de Oliveira, L. P. Z.; Castro, A. A. N.; Neumann, R.; de Oliveira, L. F. C.; Edwards, H. G. M.; Sant'Ana, A. C. The Structure of Different Cellulosic Fibres Characterized by Raman Spectroscopy. *Vib. Spectrosc.* **2016**, *86*, 324−330.
(67) Gierlinger, N.; Keplinger, T.; Harrington, M.; Schwanninger, M. Raman Imaging of Lignocellulosic Feedstock. *Cellulose - Biomass Conversion*; IntechOpen, 2013; Chapter 8.
(68) Lupoi, J. S.; Gjersing, E.; Davis, M. F. Evaluating Lignocellulosic Biomass, Its Derivatives, and Downstream Products with Raman Spectroscopy. *Front. Bioeng. Biotechnol.* **2015**, *3* (April), 1−18.
(69) Agarwal, U. P.; Ralph, S. A.; Reiner, R. S.; Baez, C. New Cellulose Crystallinity Estimation Method That Differentiates between Organized and Crystalline Phases. *Carbohydr. Polym.* **2018**, *190*, 262−270.

https://doi.org/10.1021/acssuschemeng.0c09342
ACS Sustainable Chem. Eng. XXXX, XXX, XXX−XXX

(70) Espinosa, E.; Sánchez, R.; Otero, R.; Domínguez-Robles, J.; Rodríguez, A. A Comparative Study of the Suitability of Different Cereal Straws for Lignocellulose Nanofibers Isolation. *Int. J. Biol. Macromol.* **2017**, *103*, 990−999.
(71) Liimatainen, H.; Sirviö, J.; Haapala, A.; Hormi, O.; Niinimäki, J. Characterization of Highly Accessible Cellulose Microfibers Generated by Wet Stirred Media Milling. *Carbohydr. Polym.* **2011**, *83* (4), 2005−2010.
(72) Feng, Y. H.; Cheng, T. Y.; Yang, W. G.; Ma, P. T.; He, H. Z.; Yin, X. C.; Yu, X. X. Characteristics and Environmentally Friendly Extraction of Cellulose Nanofibrils from Sugarcane Bagasse. *Ind. Crops Prod.* **2018**, *111*, 285−291.
(73) Moon, R. J.; Martini, A.; Nairn, J.; Simonsen, J.; Youngblood, J. Cellulose nanomaterials review: structure, properties and nanocomposites. *Chem. Soc. Rev.* **2011**, *40*, 3941.
(74) Liou, T. H.; Wu, S. J. Kinetics Study and Characteristics of Silica Nanoparticles Produced from Biomass-Based Material. *Ind. Eng. Chem. Res.* **2010**, *49* (18), 8379−8387.
(75) Sun, L.; Gong, K. Silicon-Based Materials from Rice Husks and Their Applications. *Ind. Eng. Chem. Res.* **2001**, *40* (25), 5861−5877.
(76) Bakar, R. A.; Yahya, R.; Gan, S. N. Production of High Purity Amorphous Silica from Rice Husk. *Procedia Chem.* **2016**, *19*, 189−195.
(77) Elimbinzi, E.; Nyandoro, S. S.; Mubofu, E. B.; Manayil, J. C.; Lee, A. F.; Wilson, K. Valorization of Rice Husk Silica Waste: Organo-Amine Functionalized Castor Oil Templated Mesoporous Silicas for Biofuels Synthesis. *Microporous Mesoporous Mater.* **2020**, *294*, 109868.
(78) Norsuraya, S.; Fazlena, H.; Norhasyimi, R. Sugarcane Bagasse as a Renewable Source of Silica to Synthesize Santa Barbara Amorphous-15 (SBA-15). *Procedia Eng.* **2016**, *148*, 839−846.
(79) Falk, G.; Shinhe, G. P.; Teixeira, L. B.; Moraes, E. G.; de Oliveira, A. P. N. Synthesis of Silica Nanoparticles from Sugarcane Bagasse Ash and Nano-Silicon via Magnesiothermic Reactions. *Ceram. Int.* **2019**, *45* (17), 21618−21624.
(80) Ghorbani, F.; Habibollah Younesi; Mehraban, Z.; Celik, M. S.; Ghoreyshi, A. A.; Anbia, M. Preparation and Characterization of Highly Pure Silica from Sedge as Agricultural Waste and Its Utilization in the Synthesis of Mesoporous Silica MCM-41. *J. Taiwan Inst. Chem. Eng.* **2013**, *44* (5), 821−828.

https://doi.org/10.1021/acssuschemeng.0c09342
ACS Sustainable Chem. Eng. XXXX, XXX, XXX−XXX